Generalized reflection and transmission of beams

Hui Yu, Xiaoqing Jiang,* Jianyi Yang, Wei Qi, and Minghua Wang
Department of Information Science and Electronic Engineering, Zhejiang University, Hangzhou 310027, China
(Received 15 October 2007; revised manuscript received 30 May 2008; published 19 September 2008)

We rigorously prove that when a bounded light beam is incident on an interface, a part of its plane wave components propagate according to the reverse mode of the ordinary reflection and transmission. Based on the two propagation modes, we propose the definition of the generalized reflection and transmission. With this definition, we solve the controversy about the Goos-Hänchen shift approaching the grazing incidence limit, and release the angular expansion method from the precondition which requires that the beam spread angle should not exceed the complement of the incident angle. Then the spectrum superposition effect is investigated for the incidence circumstance whose beam spread angle exceeds the complement of the incident angle.

DOI: 10.1103/PhysRevA.78.033827 PACS number(s): 42.25.Gy, 42.25.Bs

I. INTRODUCTION

The reflection of a bounded light beam has been the subject of numerous studies in the past, and people's interests about it are always focused on the nonspecular phenomena in the reflection. The nonspecular phenomena, namely, the differences between actual reflected beams and those predicted by geometrical optics, generally include four effects: the lateral shift, the focal shift, the angular shift, and the beam waist modification effect [1]. The four nonspecular effects have been comprehensively investigated for various multilayered structures [2–8], and for many special incident angles (such as the Brewster angle [9], the critical angle [2,10], and the resonant angle [11,12]). As much attention has been directed to light propagation rules in various novel media recently: beam reflections in negative permittivity media, negatively refractive media, and left-handed materials have also been discussed in detail [13–17].

A method prevalently utilized in these studies is the angular expansion method: the incident beam is regarded as a collection of plane waves with different propagation directions by the Fourier transform. These component waves undergo different phase and amplitude changes after the reflection, and then sum to form the reflected beam. However, a precondition of utilizing the angular expansion method to study the beam reflection is that the spread angle of the incident beam should not exceed the complement of the incident angle [18]. We can examine this precondition in Fig. 1, which depicts the incidence of a one-dimensional (uniform in y direction) TE polarized Gaussian beam on an interface between two media. The incident field is assumed to be monochromatic with an angular frequency of ω_1. The media on both sides of the interface are nonmagnetic, transparent, homogeneous, and isotropic; their refractive indexes are n_1 and n_2. The field distribution of the incident beam on the launch plane $z=0$ is $\exp(-x^2/w^2)$ [the time dependence $\exp(-i\omega_1 t)$ is suppressed here], then the spatial frequency spectrum of the incident beam is $f(k_x)=\sqrt{\pi}w\exp(-w^2k_x^2/4)$. Here w and k_x are the waist width of the Gaussian beam and the transverse wave vector, respectively. As shown in Fig. 1, the symbols θ and θ_0 denote the beam spread angle and the complement of the incident angle, respectively. Since the plane wave components whose transverse wave vectors exceed $k_0n_1\sin\theta_0$ do not propagate toward the interface (k_0 is the wave vector in vacuum), we cannot directly apply Fresnel's laws to describing the interactions between these wave components and the interface. To avoid this problem, the precondition $\theta<\theta_0$ is required to be satisfied. Under this precondition the inequality $f(k_0n_1\sin\theta_0)<f(k_0n_1\sin\theta)\approx f(0)/e$ stands, which implies that the plane wave components with $k_x>k_0n_1\sin\theta_0$ are insignificant. However, setting the precondition of $\theta<\theta_0$ does not solve the problem radically.

In fact, the unawareness of the interaction manner between a part of plane waves and the interface has caused some problems. A typical one is Lloyd's mirror. Generally the precondition $\theta<\theta_0$ is not satisfied for Lloyd's mirror, so people cannot deduce the exact distribution of its output field. Any investigations about it only rely on ray optics to determine the propagation directions of the fringes [19,20]. Another problem is the controversy about the Goos-Hänchen (GH) shift in the limit of grazing incidence, which has not received a final result so far. In this paper, we solve these problems radically by proposing the definition of the gener-

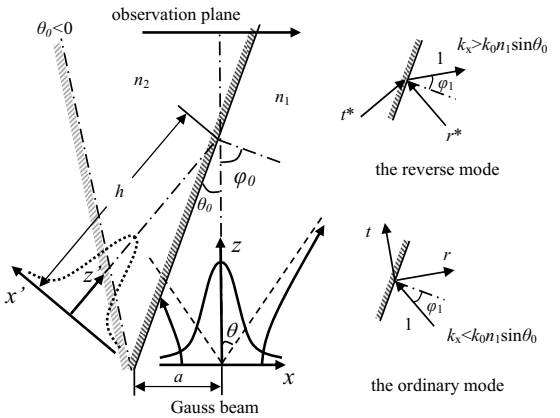

FIG. 1. Schematic diagram of the incidence of a one-dimensional Gaussian beam.

*Corresponding author; iseejxq@zju.edu.cn

 ©2008 The American Physical Society

alized reflection and transmission. The paper is organized in the following manner. First, in Sec. II we indicate that the plane wave components with $k_x > k_0 n_1 \sin\theta_0$ propagate according to the reverse mode of the ordinary reflection and transmission. Then, in Sec. III, we prove this point rigorously, and ultimately derive the expression of the output field which holds true for the incidence circumstance $\theta > \theta_0$ [Eq. (28) in Sec. III]. In Sec. IV, we discuss the GH shift in the limit of grazing incidence based on the definition of the generalized reflection. Besides the generalized reflection and transmission manner, another remarkable characteristic of the incidence circumstance $\theta > \theta_0$ is its spectrum superposition effect. This effect is also investigated in Sec. IV.

II. GENERALIZED REFLECTION AND TRANSMISSION

The ordinary reflection and transmission of the plane wave are depicted in Fig. 1, where r and t denote the reflection and the transmission coefficients determined by Fresnel's laws, respectively. According to the principle of reversibility, the reverse mode of the ordinary reflection and transmission also satisfies Maxwell's equations and the boundary conditions on the interface. The reverse mode is also presented in Fig. 1, where the asterisk denotes complex conjugate. For a long time no actual physical process has been found to correspond to it except in the deduction of the Stokes relation [21]. In fact, the reverse mode is just the manner in which the interface acts on the plane wave components with $k_x > k_0 n_1 \sin\theta_0$. We will prove this point in Sec. III. The ordinary mode plus the reverse mode cover the propagation behaviors of all plane wave components. Therefore they form the manner of the generalized reflection and transmission together. The expressions of the generalized reflection and transmission coefficients for the interface in Fig. 1 are

$$R_g(k_x) = \begin{cases} \dfrac{n_1\cos\varphi_1 - \sqrt{n_2^2 - (n_1\sin\varphi_1)^2}}{n_1\cos\varphi_1 + \sqrt{n_2^2 - (n_1\sin\varphi_1)^2}}, & k_x < k_0 n_1 \sin\theta_0 \\ \left[\dfrac{n_1\cos\varphi_1 - \sqrt{n_2^2 - (n_1\sin\varphi_1)^2}}{n_1\cos\varphi_1 + \sqrt{n_2^2 - (n_1\sin\varphi_1)^2}}\right]^*, & k_x > k_0 n_1 \sin\theta_0, \end{cases} \tag{1}$$

$$T_g(k_x) = \begin{cases} \dfrac{2n_1\cos\varphi_1}{n_1\cos\varphi_1 + \sqrt{n_2^2 - (n_1\sin\varphi_1)^2}}, & k_x < k_0 n_1 \sin\theta_0 \\ \left[\dfrac{2n_1\cos\varphi_1}{n_1\cos\varphi_1 + \sqrt{n_2^2 - (n_1\sin\varphi_1)^2}}\right]^*, & k_x > k_0 n_1 \sin\theta_0, \end{cases} \tag{2}$$

where $\varphi_1(k_x)$ is the generalized incidence angle of the plane wave component,

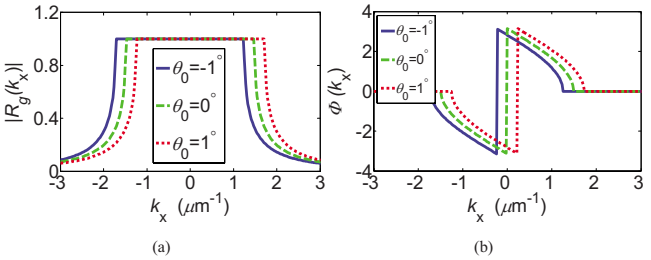

FIG. 2. (Color online) (a) Amplitude and (b) phase distributions of the generalized reflection coefficient $R_g(k_x)$. The parameters in the calculation are $n_1 = 3.37$, $n_2 = 3.35$, and $\lambda = 1.55$ μm.

$$\varphi_1(k_x) = \begin{cases} \pi - \arccos\dfrac{k_x}{k_0 n_1} - \theta_0, & k_x < k_0 n_1 \sin\theta_0 \\ \arccos\dfrac{k_x}{k_0 n_1} + \theta_0, & k_x > k_0 n_1 \sin\theta_0. \end{cases} \tag{3}$$

Amplitude and phase distributions of $R_g(k_x)$ are plotted in Fig. 2 for several different values of θ_0. Here the negative value of θ_0 means that the interface inclines to the left as shown in Fig. 1, and then the incident beam axis intersects with the interface in its inverse extension line. In Fig. 2, the generalized reflection coefficient $R_g(k_x)$ is a bandpass filtering function whose center frequency is located at $k_0 n_1 \sin\theta_0$. Its amplitude and phase are symmetrical and antisymmetrical with respect to $k_0 n_1 \sin\theta_0$, respectively. Changing the incident angle φ_0 does not affect the profile of $R_g(k_x)$, it just alters the position of the symmetrical center and then shifts $R_g(k_x)$ wholly. If the precondition $\theta < \theta_0$ is satisfied, the center frequency of $R_g(k_x)$ is far away from the distribution region of $f(k_x)$, so all significant plane wave components propagate according to the ordinary reflection and transmission.

III. ANALYTICAL JUSTIFICATION

In this section, we give a rigorous justification about the generalized reflection and transmission proposed in Sec. II. Carniglia and Mandel have rigorously proved that in a half-space which is filled with two nonmagnetic, transparent, homogeneous and isotropic media as shown in Fig. 3, an arbitrary source-free optical field can be represented by the combination of possible right incident and left incident modes [22]. If TE and TM polarizations are considered, elementary interface modes can be divided into four types: ξ_L^{TE}, ξ_L^{TM}, ξ_R^{TE}, and ξ_R^{TM}. They form a set of complete orthogonal basis in the half space. Here the suffixes L and R indicate the incidences from the left and the right, respectively. As shown in Fig. 3, each mode consists of a triplet of waves, which are the incident wave, the reflected wave, and the transmitted wave: $\xi_L^{TE/TM} = \xi_L^I + \xi_L^R + \xi_L^T$, $\xi_R^{TE/TM} = \xi_R^I + \xi_R^R + \xi_R^T$. Since the incident Gaussian beam is assumed to be TE polarized without losing the generality, we only need to consider two mode types, namely, ξ_L^{TE} and ξ_R^{TE}.

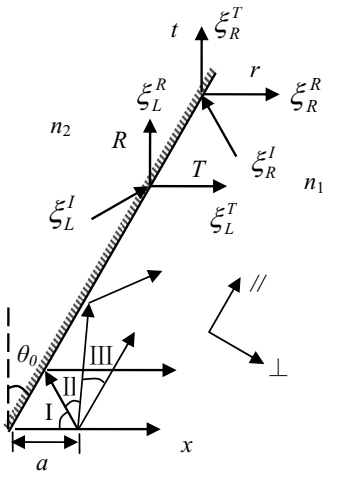

FIG. 3. Interface modes in a half-space formed by the combination of two mediums.

Since we utilize the internal coordinates of the incident beam (the x-z coordinates) here, the expressions of ξ_L^I, ξ_L^R, ξ_L^T, ξ_R^I, ξ_R^R, and ξ_R^T are a little different from those in Carniglia and Mandel's work, which utilize the coordinates along and normal to the interface,

$$\xi_L^I = \begin{cases} \frac{1}{n_2}\exp[iK_x^I(x+a)+iK_z^I z]\frac{n_2}{n_1}\sqrt{\frac{k_\perp^T}{K_\perp^I}} & \text{for } x < z\tan\theta_0 - a \\ 0 & \text{for } x > z\tan\theta_0 - a, \end{cases} \tag{4}$$

$$\xi_L^R = \begin{cases} \frac{R}{n_2}\exp[iK_x^R(x+a)+iK_z^R z]\frac{n_2}{n_1}\sqrt{\frac{k_\perp^T}{K_\perp^I}} & \text{for } x < z\tan\theta_0 - a \\ 0 & \text{for } x > z\tan\theta_0 - a, \end{cases} \tag{5}$$

$$\xi_L^T = \begin{cases} \frac{T}{n_2}\exp[ik_x^T(x+a)+ik_z^T z]\frac{n_2}{n_1}\sqrt{\frac{k_\perp^T}{K_\perp^I}} & \text{for } x > z\tan\theta_0 - a \\ 0 & \text{for } x < z\tan\theta_0 - a, \end{cases} \tag{6}$$

$$\xi_R^I = \begin{cases} \frac{1}{n_1}\exp[ik_x^I(x+a)+ik_z^I z] & \text{for } x > z\tan\theta_0 - a \\ 0 & \text{for } x < z\tan\theta_0 - a, \end{cases} \tag{7}$$

$$\xi_R^R = \begin{cases} \frac{r}{n_1}\exp[ik_x^R(x+a)+ik_z^R z] & \text{for } x > z\tan\theta_0 - a \\ 0 & \text{for } x < z\tan\theta_0 - a, \end{cases} \tag{8}$$

$$\xi_R^T = \begin{cases} \frac{t}{n_1}\exp[iK_x^T(x+a)+iK_z^T z] & \text{for } x < z\tan\theta_0 - a \\ 0 & \text{for } x > z\tan\theta_0 - a. \end{cases} \tag{9}$$

In Eqs. (4)–(9), we denote the wave vectors inside the mediums on the right and on the left of the interface by k and K, respectively. As shown in Fig. 3, R and T denote the reflection and the transmission coefficients of the left incident mode, respectively, while r and t denote the reflection and the transmission coefficients of the right incident mode, respectively. The position of the interface is determined by the parameter a, $\perp$ and $\parallel$ denote the directions normal and parallel to the interface, respectively. Although the left incident mode ξ_L^{TE} contains three waves with different propagation directions, they are related by the Fresnel law, so we choose to label a left incident mode by the wave vector of its transmitted wave $\xi_L^{TE}(k_x^T, k_z^T)$. Analogically, we choose to label a right incident mode by the wave vector of its incident wave $\xi_R^{TE}(k_x^I, k_z^I)$. The difference between the coefficients in Eqs. (4)–(6) and those in Eqs. (7)–(9) is for the requirement of the normalization as will be shown following.

Before using the interface modes listed in Eqs. (4)–(9) to represent an arbitrary field, we should prove their orthonormality in the x-z coordinates at first. According to Carniglia and Mandel's derivation [22], for the expressions listed in Eqs. (4)–(6), we have

$$\int [\xi_L^{TE}(k_x^T, k_z^T)] * \xi_L^{TE}(k_x'^T, k_z'^T) n^2(x,z)\,dx\,dz = (2\pi)^2 \delta(K_\perp^I - K_\perp'^I)\,\delta(K_\parallel^I - K_\parallel'^I)\left(\frac{n_2}{n_1}\right)^2 \frac{k_\perp^T}{K_\perp^I}. \tag{10}$$

With the help of the relations $\delta(K_\perp^I - K_\perp'^I) = (n_1/n_2)^2 (K_\perp^I / k_\perp^T)\,\delta(k_\perp^T - k_\perp'^T)$ [22] and $K_\parallel^I = k_\parallel^T$, the result of the integral in Eq. (10) is $(2\pi)^2 \delta(k_\perp^T - k_\perp'^T)\,\delta(k_\parallel^T - k_\parallel'^T)$. Since $k_\perp^T$ and $k_\parallel^T$ can be expressed in terms of k_x^T and k_z^T, namely, $k_\perp^T = k_x^T \cos\theta_0 - k_z^T \sin\theta_0$ and $k_\parallel^T = k_x^T \sin\theta_0 + k_z^T \cos\theta_0$, we can deduce the following relation: $\delta(k_\perp^T - k_\perp'^T)\,\delta(k_\parallel^T - k_\parallel'^T) = \delta(k_x^T - k_x'^T)\,\delta(k_z^T - k_z'^T)$. Then the ultimate integral result of Eq. (10) is

$$\int [\xi_L^{TE}(k_x^T, k_z^T)]^* \xi_L^{TE}(k_x'^T, k_z'^T) n^2(x,z)\,dx\,dz = (2\pi)^2 \delta(k_x^T - k_x'^T)\,\delta(k_z^T - k_z'^T). \tag{11}$$

For the right incident mode listed in Eqs. (7)–(9), we have

$$\int [\xi_R^{TE}(k_x^I, k_z^I)]^* \xi_R^{TE}(k_x'^I, k_z'^I) n^2(x,z)\,dx\,dz = (2\pi)^2 \delta(k_\perp^I - k_\perp'^I)\,\delta(k_\parallel^I - k_\parallel'^I) = (2\pi)^2 \delta(k_x^I - k_x'^I)\,\delta(k_z^I - k_z'^I). \tag{12}$$

Having proved the orthonormality of the right and the left incident modes listed in Eqs. (4)–(9), we can use them to present an arbitrary TE polarized source-free optical field in the half-space shown in Fig. 3.

$$E(x,z,t) = \frac{1}{(2\pi)^2}\iint_{K_\perp^I>0} \exp(-i\omega t) f_1(k_x^T,k_z^T)\xi_L^{TE}(k_x^T,k_z^T)dk_x^T dk_z^T + \frac{1}{(2\pi)^2}\iint_{k_\perp^I<0} \exp(-i\omega t) f_2(k_x^I,k_z^I)\xi_R^{TE}(k_x^I,k_z^I)dk_x^I dk_z^I. \tag{13}$$

In Eq. (13), ω is the angular frequency of the interface mode, $(n\omega/c)^2=k_x^2+k_z^2$, where c is the light velocity in vacuum. On taking products of both sides of Eq. (13) with $n^2(x,z)[\xi_L^{TE}(k_x'^T,k_z'^T)]^*$ and integrating over all space, with the aid of Eq. (11) we find

$$f_1(k_x'^T,k_z'^T) = \exp(i\omega' t)\int_{-\infty}^{+\infty} n^2(x,z)E(x,z,t) \times [\xi_L^{TE}(k_x'^T,k_z'^T)]^* dxdz. \tag{14}$$

Similarly we have

$$f_2(k_x'^I,k_z'^I) = \exp(i\omega' t)\int_{-\infty}^{+\infty} n^2(x,z)E(x,z,t)[\xi_R^{TE}(k_x'^I,k_z'^I)]^* dxdz. \tag{15}$$

Since we discuss the monochromatic field here, $E(x,z,t)=e(x,z)\exp(-i\omega_1 t)$, the space integrals in Eqs. (14) and (15) only need to be conducted on the plane $z=0$.

$$f_1(k_x'^T) = \int_{-\infty}^{+\infty} n^2(x,z)e(x,0)[\xi_L^{TE}(k_x'^T,k_z'^T)]^* dx, \tag{16}$$

$$f_2(k_x'^I) = \int_{-\infty}^{+\infty} n^2(x,z)e(x,0)[\xi_R^{TE}(k_x'^I,k_z'^I)]^* dx. \tag{17}$$

Before calculating the integrals in Eqs. (16) and (17), we assume that $n_1>n_2$. Since the incident beam is located on the right of the interface, and there is only the transmitted wave in this region for the left incident mode ξ_L^{TE}, we have

$$f_1(k_x'^T) = \int_{-\infty}^{+\infty} n_1 e(x,0)\exp[-ik_x'^T(x+a)]\left(T\sqrt{\frac{k_\perp'^T}{K_\perp'^I}}\right)^* dx = n_1 T\sqrt{\frac{k_\perp'^T}{K_\perp'^I}}\exp(-ik_x'^T a)f(k_x'^T). \tag{18}$$

In Eq. (18), $f(k_x'^T)$ is the Fourier transform of $e(x,0)$; the variation range of $k_x'^T$ is $\{k_0 n_1\cos[\arcsin(n_2/n_1)-\theta_0], k_0 n_1\}$. Since $k_\perp'^T$ is a real number for the incidence from an optically thinner medium to an optically denser medium, the conjugate symbol * in Eq. (18) can be removed.

As the right incident mode contains the incident and the reflected waves on the right of the interface, the integral in Eq. (17) includes two terms,

$$f_2(k_x'^I) = \int_{-\infty}^{+\infty} n_1^2 e(x,0)[\xi_R^I(k_x'^I,k_z'^I)]^* dx + \int_{-\infty}^{+\infty} n_1^2 e(x,0)[\xi_R^R(k_x'^R,k_z'^R)]^* dx. \tag{19}$$

The two integrals in Eq. (19) need to be conducted according to three regions of $k_x'^I$ as shown in Fig. 3.

Region I. $k_x'^I \in (-k_0 n_1, -k_0 n_1\cos 2\theta_0)$. The incident wave with $k_x'^I=-k_0 n_1\cos 2\theta_0$ gives rise to a reflected wave propagating along the positive direction of the x axis as shown in Fig. 3. For the right incident modes ξ_R^{TE} in region I, their reflected waves propagate downwards $k_z'^R<0$, so the second integral in Eq. (19) can be discarded.

$$f_2(k_x'^I) = \int_{-\infty}^{+\infty} n_1^2 e(x,0)[\xi_R^I(k_x'^I,k_z'^I)]^* dx = n_1\exp(-ik_x'^I a)f(k_x'^I). \tag{20}$$

Region II. $k_x'^I \in \{-k_0 n_1\cos 2\theta_0, k_0 n_1\sin[\arcsin(n_2/n_1)+\theta_0-\pi/2]\}$, and then $k_x'^R \in \{k_0 n_1\cos[\arcsin(n_2/n_1)-\theta_0], k_0 n_1\}$. The transverse wave vector of the wave incident at the critical angle is $k_0 n_1\sin[\arcsin(n_2/n_1)+\theta_0-\pi/2]$. For the right incident modes in region II, their incident angles are smaller than the critical angle, and their reflected waves propagate upward $k_z'^R>0$. Substituting Eqs. (7) and (8) into Eq. (19) and noting that $r=r^*$ for the partial reflection, we have

$$f_2(k_x'^I) = n_1\exp(-ik_x'^I a)f(k_x'^I) + n_1 r\exp(-ik_x'^R a)f(k_x'^R). \tag{21}$$

It is important to note that the variation range of $k_x'^R$ here is the same as that of $k_x'^T$ in Eq. (18).

Region III. $k_x'^I \in \{k_0 n_1\sin[\arcsin(n_2/n_1)+\theta_0-\pi/2], k_0 n_1\sin\theta_0\}$, and $k_x'^R \in \{k_0 n_1\sin\theta_0, k_0 n_1\cos[\arcsin(n_2/n_1)-\theta_0]\}$. Incident angles of the right incident modes in this region exceed the critical angle, thus the expression of $f_2(k_x'^I)$ is

$$f_2(k_x'^I) = n_1\exp(-ik_x'^I a)f(k_x'^I) + n_1 r^*\exp(-ik_x'^R a)f(k_x'^R). \tag{22}$$

Having calculated the amplitudes of all possible component modes, we can express an optical field in terms of their superposition. With the aid of Eqs. (18)–(22), we have

$$e(x,z) = \frac{1}{2\pi}\int_{-k_0 n_1}^{k_0 n_1 \sin\theta_0} n_1 \exp(-ik_x'^I a) f(k_x'^I)\xi_R^{TE}(k_x'^I)dk_x'^I + \frac{1}{2\pi}\int_{k_0 n_1 \sin\theta_0}^{k_0 n_1 \cos[\arcsin(n_2/n_1)-\theta_0]} n_1 r^* \exp(-ik_x'^R a) f(k_x'^R)\xi_R^{TE}(k_x'^I)dk_x'^R + \frac{1}{2\pi}\int_{k_0 n_1 \cos[\arcsin(n_2/n_1)-\theta_0]}^{k_0 n_1} n_1 r \exp(-ik_x'^R a) f(k_x'^R)\xi_R^{TE}(k_x'^I)dk_x'^R + \frac{1}{2\pi}\int_{k_0 n_1 \cos[\arcsin(n_2/n_1)-\theta_0]}^{k_0 n_1} n_1 T\sqrt{\frac{k_\perp'^T}{K_\perp'^I}} \exp(-ik_x'^T a) f(k_x'^T)\xi_L^{TE}(k_x'^T)dk_x'^T. \tag{23}$$

It is evident that the first integral in Eq. (23) implies the ordinary reflection and transmission, thus we need to examine the last three integrals.

Since the integrating range of the second integral of Eq. (23) is region III, where the incident angle is bigger than the critical angle, we have $rr^*=|r|^2=1$ and $r^*t=t^*$. Then substituting the expression of ξ_R^{TE} into its integrand, we have

$$n_1 r^* \exp(-ik_x'^R a) f(k_x'^R)\xi_R^{TE}(k_x'^I) = \begin{cases} r^* f(k_x'^R)\exp[ik_x'^I x + ik_z'^I z + i(k_x'^I - k_x'^R)a] + f(k_x'^R)\exp(ik_x'^R x + ik_z'^R z), & x > z\tan\theta_0 - a \\ t^* f(k_x'^R)\exp[iK_x'^T x + iK_z'^T z + i(K_x'^T - k_x'^R)a], & x < z\tan\theta_0 - a. \end{cases} \tag{24}$$

Since it is the evanescent wave on the left of the interface for region III, the implication of Eq. (24) is just the reverse mode shown in Fig. 1.

The last two integrals of Eq. (23) can be merged since they have the identical integrating range, then the integrand of the merged integral is

$$n_1 r \exp(-ik_x'^R a) f(k_x'^R)\xi_R^{TE}(k_x'^I) + n_1 T\sqrt{\frac{k_\perp'^T}{K_\perp'^I}} \exp(-ik_x'^T a) f(k_x'^T)\xi_L^{TE}(k_x'^T) = \begin{cases} T\dfrac{k_\perp'^T}{K_\perp'^I} f(k_x'^T)\exp[iK_x'^I x + iK_z'^I z + i(K_x'^I - k_x'^T)a] + RT\dfrac{k_\perp'^T}{K_\perp'^I} f(k_x'^T)\exp[iK_x'^R x + iK_z'^R z + i(K_x'^R - k_x'^T)a] \\ + trf(k_x'^R)\exp[iK_x'^T x + iK_z'^T z + i(K_x'^T - k_x'^R)a], \quad x < z\tan\theta_0 - a \\ rf(k_x'^R)\exp[ik_x'^I x + ik_z'^I z + i(k_x'^I - k_x'^R)a] + r^2 f(k_x'^R)\exp(ik_x'^R x + ik_z'^R z) + T^2\dfrac{k_\perp'^T}{K_\perp'^I} f(k_x'^T)\exp(ik_x'^T x + ik_z'^T z), \quad x > z\tan\theta_0 - a. \end{cases} \tag{25}$$

In Eq. (25), $K_x'^T = K_x'^R$, $k_x'^T = k_x'^R$, $K_z'^T = K_z'^R$, and $k_z'^T = k_z'^R$. Utilizing the relations $RTk_\perp'^T/K_\perp'^T + rt = Rt + rt = 0$ and $r^2 + T^2 k_\perp'^T/K_\perp'^T = r^2 + Tt = 1$, and then noting that both r and t are real numbers for the partial reflection, we can reorganize Eq. (25) into the following form:

$$n_1 r \exp(-ik_x'^R a) f(k_x'^R)\xi_R^{TE}(k_x'^I) + n_1 T\sqrt{\frac{k_\perp'^T}{K_\perp'^I}} \exp(-ik_x'^T a) f(k_x'^T)\xi_L^{TE}(k_x'^T) = \begin{cases} t^* f(k_x'^R)\exp[iK_x'^I x + iK_z'^I z + i(K_x'^I - k_x'^R)a], & x < z\tan\theta_0 - a \\ r^* f(k_x'^R)\exp[ik_x'^I x + ik_z'^I z + i(k_x'^I - k_x'^R)a] + f(k_x'^R)\exp(ik_x'^R x + ik_z'^R z), & x > z\tan\theta_0 - a. \end{cases} \tag{26}$$

The same as Eq. (24), Eq. (26) also means the reverse mode shown in Fig. 1.

With Eqs. (23), (24), and (26), we come to the conclusion given in Sec. II. After the angular expansion, the plane wave components with $k_x > k_0 n_1 \sin\theta_0$ propagate as the reverse mode of the ordinary reflection and transmission, so the expression of the field on the right of the interface is

$$e(x,z) = \frac{1}{2\pi}\int_{-k_0 n_1}^{k_0 n_1} f(k_x)\exp(ik_x x + i\sqrt{k_0^2 n_1^2 - k_x^2}z)dk_x + \frac{1}{2\pi}\int_{-k_0 n_1}^{k_0 n_1} f(k_x)R_g(k_x)\exp[ik_x^{Rg}x + i\sqrt{k_0^2 n_1^2 - (k_x^{Rg})^2}z + i(k_x^{Rg} - k_x)a]dk_x. \tag{27}$$

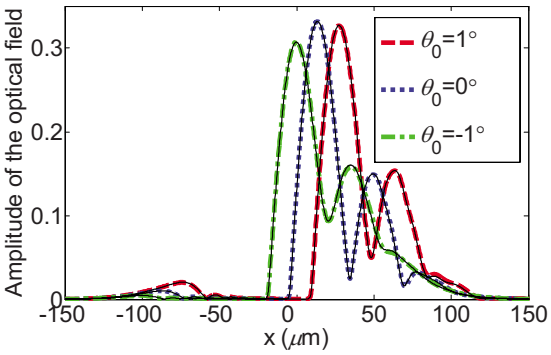

FIG. 4. (Color online) Field distributions on a certain z plane when a beam is incident on a dielectric slab with different values of θ_0. Nonsolid and solid lines correspond to theoretical calculations and simulations, respectively. Thickness and refractive index of the slab are 4 μm and 3.35, respectively. The refractive index of the medium surrounding the slab is 3.37. Other parameters in the calculations are $\lambda=1.55$ μm, $w=2$ μm, $a=2w$, $z=800$ μm, and $\theta=4.18°$.

In Eq. (27), the symbol k_x^{Rg} denotes the transverse wave vector of the generalized reflected wave, and the two integrals represent the incident and the reflected fields. Equation (27) can be reorganized into the following form that we are familiar with:

$$e(x,z)=\frac{1}{2\pi}\int_{-k_0n_1}^{k_0n_1} f(k_x)\exp(ik_xx+i\sqrt{k_0^2n_1^2-k_x^2}z)dk_x + \frac{1}{2\pi}\int_{-k_0n_1}^{k_0n_1} f(k_x)R_g(k_x)\exp(ik_xx'+i\sqrt{k_0^2n_1^2-k_x^2}z')dk_x, \tag{28}$$

where (x,z) and (x',z') are the intrinsic coordinate system of the incident beam and its mirror-reflected coordinates, respectively.

Though our proof is based on the interface with a refractive index distribution of $n_1>n_2$, an analogical deduction and result hold true for the case of $n_2>n_1$ and for various multilayered structures. As an illustration, we calculate field distributions on a certain z plane when a beam is incident on a dielectric slab with different values of θ_0. The results are shown in Fig. 4, where they are compared with simulations utilizing the beam propagation method (BPM) [23]. The parameters in Fig. 4 assure that $\theta>\theta_0$, so considerable plane wave components are handled by the reversed mode shown in Fig. 1. The agreement between theoretical calculations and simulations validates further the generalized reflection and transmission theory.

IV. GH SHIFT IN THE INCIDENCE CIRCUMSTANCE $\theta>\theta_0$

With the definition of the generalized reflection coefficient $R_g(k_x)$, we can discuss the GH shift in the limit of grazing incidence ($\varphi_0=90°$) [24]. There is an unsolved controversy about this problem. Lotsch [24] and Renard [25] thought that the GH shift for this case did not exist. Utilizing the angular expansion method, Mcguirk [18] asserted that the shift was not zero. However, he failed to prove it rigorously. By assuming an incident beam with a sufficiently small spread angle θ (assure $\theta_0>\theta$), he could derive the GH shift for incident angles arbitrarily close to 90°. However, he could not give a reasonable explanation about the GH shift at $\varphi_0=90°$ or that under the incidence condition $\theta>\theta_0$. According to the theory of the angular expansion method, the GH shift can be regarded as the first order derivative of the phase of the reflectance at the position $k_x=0$,

$$D=\left.\frac{d\phi}{dk_x}\right|_{k_x=0}, \tag{29}$$

where $\phi(k_x)$ is the phase of $R_g(k_x)$. As we have indicated, the traditional reflection and transmission coefficients are defined in the domain $(-\infty,k_0n_1\sin\theta_0)$, so $k_x=k_0n_1\sin\theta_0$ is a discontinuity point. When φ_0 is 90°, this discontinuity point is located at the position $k_x=0$, thus the differentiation in Eq. (29) is meaningless. For the incidence condition $\theta>\theta_0$, it is unable to deduce the exact expression of the reflected beam without the generalized reflection coefficient, so the GH shift also cannot get a reasonable explanation.

Our work has extended the definition domain of the reflectance to the entire k_x axis, so we can examine the derivability of $\phi(k_x)$ at its center frequency $k_x=k_0n_1\sin\theta_0$. As shown in Fig. 2(b), $\phi(k_x)$ is antisymmetrical about its center frequency, meanwhile its left and right limits at this position are $-\pi$ and π, respectively. Since $-\pi$ and π denote the same angle actually, $\phi(k_x)$ is continuous and derivable at $k_x=k_0n_1\sin\theta_0$. When $\varphi_0=90°$, the derivative in Eq. (29) does exist. For example, its value is -1.36 μm for the parameters in Fig. 2. In fact, the incident angle of 90° ($\theta_0=0°$) should not be regarded as the incidence limit. As shown in Figs. 1 and 4, a beam can also be incident on the interface with negative values of θ_0 due to the beam spreading.

Besides the generalized reflectance $R_g(k_x)$, the output field on the right of the interface is modulated by the spectrum superposition effect in the incidence circumstance $\theta>\theta_0$. Utilizing the coordinate conversion and the paraxial approximation [7,26], we can deduce the spatial frequency spectrum which determines the optical field on the right of the interface from Eq. (28),

$$g(k_x)=\frac{1}{\cos 2\theta_0}f(k_x')\exp\{i[k_x'(z'-h)\sin 2\theta_0] + [k_0^2n_1^2-k_x'^2]^{1/2}(z'\cos 2\theta_0+2h\sin^2\theta_0)\} + f(k_x)R_g(k_x)\exp[i(k_0^2n_1^2-k_x^2)^{1/2}z']. \tag{30}$$

In Eq. (30), h is the distance from the incident position to the interface along the beam axis as shown in Fig. 1. Its value is determined by the parameter a, $h=a/\tan\theta_0$. The expression of the variable k_x' in Eq. (30) is $k_x'=(k_0n_1\sin 2\theta_0-k_x)/\cos 2\theta_0$.

The spectrum $g(k_x)$ in Eq. (30) consists of two sections. One is the reflected spectrum whose center locates at $k_x=0$. If we ignore the influence of $R_g(k_x)$, its $1/e$ half width is about $k_0n_1\sin\theta$. The other is the incident spectrum

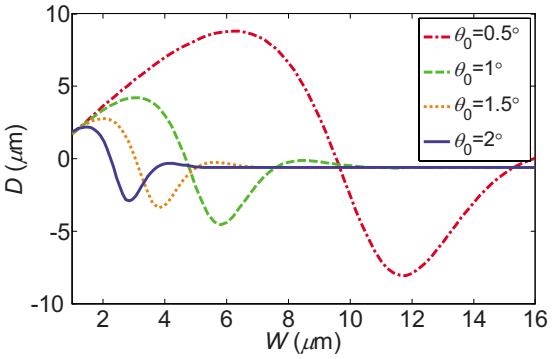

FIG. 5. (Color online) Goos-Hänchen shift as a function of the incident Gaussian beam width. The parameters in the calculations are $n_2=3.27$, $a=2w$, $z=5000$ μm; other parameters are the same as those in Fig. 2.

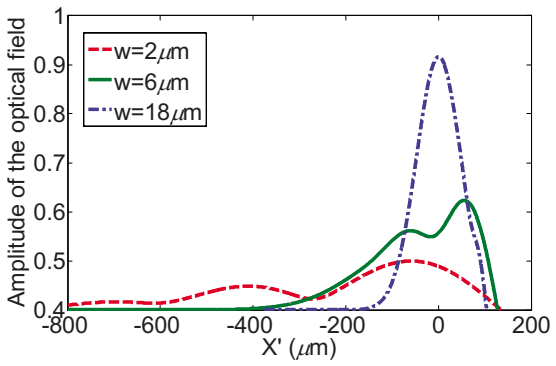

FIG. 6. (Color online) Field distributions associated with the GH shift shown in Fig. 5. In the calculation $\theta_0=1°$, other parameters are the same as those in Fig. 5.

after the coordinate conversion. Its center is located at $k_x=k_0n_1\sin 2\theta_0$, and its $1/e$ half width is $k_0n_1\sin\theta\cos 2\theta_0$. For the ordinary incidence that $\theta_0 \gg \theta$, there is no overlapping between the two spectrums since $k_0n_1\sin 2\theta_0 > k_0n_1\sin\theta\cos 2\theta_0 + k_0n_1\sin\theta$. When we conduct the inverse Fourier transform to $g(k_x)$ to calculate the field on the right of the interface, the main contribution to the integral comes from the integrating domain $(-\infty, k_0n_1\sin\theta_0)$ in the far field. It is the reflected spectrum occupying this domain, so the output field on the right of the interface can be regarded as a pure reflected field in the far field. On the contrary, if $\theta > \theta_0$, the reflected and the incident spectrums superpose with each other, which is called the spectrum superposition effect in this paper. Then in the real space, it appears that the output field is the interference of the incident beam and its virtual image. In Fig. 4, since the distance between the incident beam and its image is fixed ($a=2w$), the output fields exhibit the similar fringes for different values of θ_0.

Due to the spectrum superposition effect, we can no longer use Eq. (29) to calculate the GH shift of the output field in the incidence circumstance $\theta > \theta_0$. Its exact definition should be

$$D = \left. \frac{d\{\text{angle}(g(k_x)/f(k_x)/\exp(i\sqrt{k_0^2n_1^2 - k_x^2}z'))\}}{dk_x} \right|_{k_x=0}. \tag{31}$$

Plots of the value of D versus the waist width of the incident Gaussian beam are shown in Fig. 5, where negative values of D correspond to GH shifts toward the positive direction of the x' axis. It is well known that the GH shift is independent of the incident beam width for the ordinary incidence. However, this conclusion does not stand when $\theta > \theta_0$ as shown in Fig. 5. Another interesting phenomenon is the negative GH shift (the positive value of D) when the value of w is small. As w increases, the condition $\theta > \theta_0$ is not satisfied anymore and thus the spectrum superposition effect is eliminated. Finally, the value of D levels off at a negative value which can be calculated by Eq. (29). Figure 6 presents field distributions associated to the GH shift shown in Fig. 5. The abscissas of output peaks are −57.9, 55.9, and 0.62 μm for $w=2$, 6, and 18 μm, respectively. We find the locations of output peaks in Fig. 6 differ from the GH shifts in Fig. 5 except for the case of $w=18$ μm. The reason is that besides the GH shift, the position of the output peak is also influenced by the angular shift and the focal shift induced by the spectrum superposition effect [1,7].

At the end of this section, we give a simple discussion about the feasibility of the experimental test. In experiment, we can measure the positions of the output peaks at different propagation distances, and then determine their linear relation by data fitting $x'=az'+b$. In theory, the position of the output peak is determined by the equation $x'=\alpha(z'+\gamma)+\beta$. The symbols α, β, and γ denote the angular shift, the GH shift, and the focal shift, respectively. All of them can be determined by strict theoretical calculation [7]. Comparing the practical testing result with the theoretical calculation, we can validate the result in Fig. 5.

V. CONCLUSION

When a bounded beam is incident on an interface, part of its plane wave components do not propagate toward the interface after the angular expansion. In this paper, by representing an optical field in terms of the interface modes which form a set of complete orthogonal basis, we rigorously prove that these plane waves propagate according to the reverse mode of the ordinary reflection and transmission. Based on the two interaction manners between different plane wave components and the interface, we propose the definition of the generalized reflection and transmission. With this definition, we solve the controversy about the GH shift in the grazing incidence limit, and remove one precondition of utilizing the angular expansion method, namely, the value of θ_0 should exceed that of θ. Then the characteristics of the incidence circumstance $\theta > \theta_0$ are studied, including the spectrum position effect and the GH shift of the output field.

In fact, the incidence circumstance $\theta > \theta_0$ has other applications besides Lloyd's mirror. A typical one is the total-internal-reflection (TIR) optical waveguide switch in the area of integrated optics. The waveguide width is on the scale of

several microns for practical TIR switches, while the crossing angle between the incident waveguide and the electrode seldom exceeds 3°, so the inequality $\theta > \theta_0$ is always satisfied. Our work gives a theoretical foundation for studying these light propagation problems.

ACKNOWLEDGMENTS

This work was supported by the Key Fund of Natural Science Foundation of China (Grant No. 60436020) and the Major State Basic Research Development Program of China (Grant No. 2007CB613405).

[1] T. Tamir, J. Opt. Soc. Am. A **3**, 558 (1986).
[2] B. R. Horowitz and T. Tamir, J. Opt. Soc. Am. **61**, 586 (1971).
[3] T. Tamir and H. L. Bertoni, J. Opt. Soc. Am. **61**, 1397 (1971).
[4] V. Shah and T. Tamir, J. Opt. Soc. Am. **73**, 37 (1983).
[5] C. W. Hsue and T. Tamir, Opt. Commun. **49**, 383 (1984).
[6] C. W. Hsue and T. Tamir, J. Opt. Soc. Am. A **2**, 978 (1985).
[7] R. P. Riesz and R. Simon, J. Opt. Soc. Am. A **2**, 1809 (1985).
[8] W. Nasalski, T. Tamir, and L. Lin, J. Opt. Soc. Am. A **5**, 132 (1988).
[9] H. M. Lai and S. W. Chan, Opt. Lett. **27**, 680 (2002).
[10] C. C. Chan and T. Tamir, J. Opt. Soc. Am. A **4**, 655 (1987).
[11] C. F. Li, Phys. Rev. Lett. **91**, 133903 (2003).
[12] L. G. Wang, H. Chen, and S. Y. Zhu, Opt. Lett. **30**, 2936 (2005).
[13] P. R. Berman, Phys. Rev. E **66**, 067603 (2002).
[14] J. A. Kong, B. I. Wu, and Y. Zhang, Appl. Phys. Lett. **80**, 2084 (2002).
[15] I. V. Shadrivov, A. A. Zharov, and Y. S. Kivshar, Appl. Phys. Lett. **83**, 2713 (2003).
[16] D. K. Qing and G. Chen, Opt. Lett. **29**, 872 (2004).
[17] L. G. Wang and S. Y. Zhu, Appl. Phys. Lett. **87**, 221102 (2005).
[18] M. Mcguirk and C. K. Carniglia, J. Opt. Soc. Am. **67**, 103 (1977).
[19] J. Lekner, J. Opt. Soc. Am. A **13**, 1809 (1996).
[20] B. E. Allman, A. G. Klein, K. A. Nugent, and G. I. Opat, Appl. Opt. **33**, 1806 (1994).
[21] E. Hecht, *Optics* (Higher Education Press, Beijing, 2005).
[22] C. K. Carniglia and L. Mandel, Phys. Rev. D **3**, 280 (1971).
[23] R. Scarmozzino, A. Gopinath, R. Pregla, and S. Helfert, IEEE J. Sel. Top. Quantum Electron. **6**, 150 (2000).
[24] K. V. Lotsch, J. Opt. Soc. Am. **58**, 551 (1968).
[25] R. H. Renard, J. Opt. Soc. Am. **54**, 1190 (1964).
[26] H. Yu, X. Q. Jiang, J. Y. Yang, W. Qi, and M. H. Wang, Opt. Lett. **31**, 2747 (2006).